Applied Surface Science 357 (2015) 1319–1324

Contents lists available at ScienceDirect

Applied Surface Science

journal homepage: www.elsevier.com/locate/apsusc

A novel approach in controlling the conductivity of thin films using molecular layer deposition

Andrew Lushington, Jian Liu, Mohammad N. Bannis, Biwei Xiao, Stephen Lawes, Ruying Li, Xueliang Sun*

Department of Mechanical and Materials Engineering, University of Western Ontario, London, ON N6A 5B9, Canada

ARTICLE INFO

Article history:
Received 22 March 2015
Received in revised form
16 September 2015
Accepted 19 September 2015
Available online 25 September 2015

Keywords:
Hybrid inorganic–organic films
Conductive Al_2O_3
Graphite
Pyrolysis
Molecular layer deposition
Electrical conductivity

ABSTRACT

Here we present a novel way to grow aluminum alkoxide films with tunable conductivity with molecular level accuracy with the use of molecular layer deposition (MLD). Alternating exposures of trimethylaluminum (TMA), ethylene glycol (EG), and terephthaloyl chloride (TC) are used to grow the aluminium alkoxide films. Control over film composition was accomplished by alternating cycles of EG and TC between cycles of TMA and EG. In this fashion the aluminum to carbon ratio can be accurately controlled. These films were then pyrolyzed under a reducing atmosphere to yield a conductive Al2O3/carbon composite. Raman spectroscopy determined that nanocrystalline sp2-graphitic carbon was formed following pyrolysis while sheet resistance measurements determined that conductivity of the film is directly related to aluminium–carbon ratio. To further elucidate the origin of conductivity within the film, synchrotron based XPS was performed.

© 2015 Elsevier B.V. All rights reserved.

1. Introduction

Inorganic–organic hybrid films have attracted global attention due to their application in solar cells [1], electronics [2], photonics [3], sensors [4], as well as electrochemical processes [5]. Inorganic components of these hybrid films can provide desired mechanical, optical, chemical and electrical properties while the organic component provides increased flexibility and reduced density [6]. There are a number of methods for preparing inorganic–organic hybrid materials including sol–gel processes [7], use of silsequinoxanes [8], hydrothermal synthesis [9], self-assembling procedures [10], integrative synthesis [11], Langmuir-Blodget method [12], and electrodeposition [13]. Although these methods are quite versatile, they lack the ability to grow films over high aspect ratio substrates with atomic precision. An alternative method for growing hybrid inorganic–organic materials is to utilize the gas phase deposition technique of atomic layer deposition (ALD) and molecular layer deposition (MLD). ALD and MLD are chemical thin-film deposition techniques based on sequential, self-limiting surface reactions that can conformally coat high aspect ratio structures. ALD processes typically focus on inorganic materials [14], whereas MLD processes are designed to use organic reactants [15]. By mixing the process of ALD and MLD together, binary surface reactions between a metal-ligand reactant and an organic reactant can yield a hybrid inorganic–organic film. Many inorganic–organic hybrid materials have been grown using this technique including alucones [16], zincones [17], and titanicones [18]. This family of "metalcones", is prepared using an organic alcohol precursors along with an organometallic precursor to deposit the metal alkoxide polymeric films. The number of possible combinations using inorganic ALD and organic MLD reactants is extensive due to the large number of organic moieties available. However, the mixed deposition of ALD and MLD is challenging, and appropriate reactions between inorganic and organic components need to be determined.

Hybrid films are useful for a number of applications in their as-deposited state, however, they can also be used as precursors for metal oxide/carbon composites or porous metal oxide films [19]. Pyrolyzing hybrid films under inert atmospheric conditions can produce metal oxide/carbon composite films [5]. Furthermore, pyrolysis of hybrid ALD/MLD films containing nitrogen has been shown to produce N-doped metal oxides [20]. Abdulagatov et al. [5] demonstrated that the pyrolysis of titanicone films can produce conductive films. Being able to deposit thin conformal conductive films on high surface area materials has a number of key applications, especially for electrochemical devices. They attribute the conductivity of the pyrolyzed film to the formation of sp^2-graphitic

* Corresponding author.
E-mail address: xsun@eng.uwo.ca (X. Sun).

http://dx.doi.org/10.1016/j.apsusc.2015.09.155
0169-4332/© 2015 Elsevier B.V. All rights reserved.

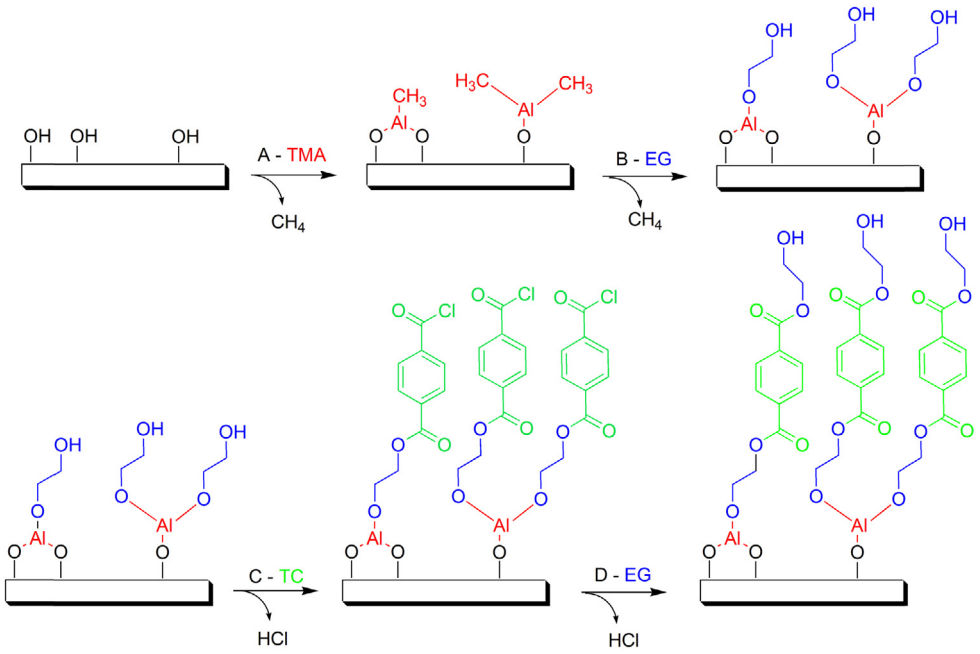

Fig. 1. Mechanism of MLD reaction between TMA, EG and TC.

carbon. However, their deposition of titanicone films contained a small amount of carbon, thus limiting the composites potential conductivity. Furthermore the effect of carbon on the metal oxide during pyrolysis was not determined.

In this paper, we describe a new MLD strategy to deposit aluminum alkoxide films with tuneable carbon content. MLD films are grown using trimethylaluminium (TMA), ethylene glycol (EG), and terephthaloyl chloride (TC). These films are pyrolyzed at various temperatures under an inert atmosphere. The effect of carbon on the metal oxide is studied by Raman analysis as well as synchrotron based XPS. To the best of our knowledge, this is the first reported process of a metalcone with tuneable carbon content.

2. Materials and methods

All hybrid inorganic–organic films were deposited in a commercial cross flow-type hot-wall ALD reactor (Arradiance Gemstar-8) using $Al(CH_3)_3$ (trimethylaluminium, TMA; Strem, 98%), $C_2H_6O_2$ (ethylene glycol, EG; Sigma–Aldrich, 99.8%), and $C_8H_4Cl_2O_2$ (terephthaloyl chloride, TC; Sigma–Aldrich, 99%). All precursors were evaporated with an external reservoir. TMA was held at room temperature (RT) while EG and TC were heated up to 90 °C in order to provide sufficient vapour pressure. Nitrogen (99.999%, Praxair) was used as both a carrier and purge gas. All depositions were conducted at 150 °C on double polished Si (1 0 0) and high purity SiO_2 glass substrates. Precursor manifolds were heated to 120 °C to ensure precursor volatility before entering the deposition chamber. An aluminum oxide seed layer of 10 nm was deposited on the substrate using TMA and H_2O. Inorganic–organic hybrid films with increased carbon content were deposited using a 50 ms pulse of TMA and EG and a 500 ms pulse of TC. After each pulse, nitrogen flow was increased to 100 sccm for 15 s to ensure all precursors reach the deposition chamber, the flow rate is then dropped to 10 sccm for 15 s to remove by-products produced during the reaction. Relatively long purge times were used to guarantee removal of excess precursor and reaction by-products.

Pyrolysis of MLD films was performed at temperatures from 600 to 1000 °C in a high temperature furnace (Lindberg/Blue M tube furnace). Silicon samples with MLD films were placed on ceramic boats which were then inserted into a quartz tube. Prior to pyrolysis, high purity Ar was allowed to flow over the substrates for 30 min to ensure an inert atmosphere was present in the tube. Samples were held at the pyrolysis temperature for 1 h as is typically done for treatment of MLD films [5].

Film thickness and surface morphology was determined by a field emission scanning electron microscope (FE-SEM, Hitachi S4800). Raman spectroscopy was obtained using a HORIBA Scientific LabRAM HR Raman spectrometer system with a 532.4 nm laser and optical microscope operating at RT. Fourier transform infrared spectroscopy (FTIR) was obtained with a Nicolet 6700 FTIR spectrometer. Aluminum 2p X-ray photoelectron spectroscopy (XPS) measurements were collected at the variable line spacing plane grating monochromator (VLS-PGM) beamline equipped with a Scienta 100 analyser at the Canadian Light Source (CLS) in Saskatoon, Saskatchewan, Canada. The CLS is a third generation synchrotron light source operating at 2.9 GeV. Electrical measurements were performed on pyrolyzed MLD films deposited on high purity SiO_2 glass. Sheet resistance measurements were carried out using a home-built four-point probe equipped with a Keithley 2400 source meter.

3. Results and discussion

Carbon content in aluminum alkoxide films is controlled by the number of ethylene glycol (EG) and terephthaloyl chloride (TC) cycles prior to a pulse of trimethylaluminium (TMA). As outlined in Fig. 1, step “A” consists of a TMA pulse while steps B and C are pulses of EG and TC, respectively. Each step is followed by an N_2 purge to remove reaction by-products. Steps “B” and “C” can be cycled to increase carbon content in the MLD film. 1 MLD cycle for films denoted as 1:1 would consist of steps “ABCB”, whereas 1 MLD cycle for a 1:3 film would be, “ABCBCBCB.” In this manner, the amount of carbon in the film can be precisely controlled. In order to insure a homogenous distribution of hydroxyl groups on the surface, a 10 nm Al_2O_3 seed layer was deposited prior to the deposition of the inorganic–organic hybrid films. Cross section SEM of silicon wafers was used to determine film thickness. As shown in Fig. 2, the produced 1:1 polymer film uniformly coats the Si substrate with

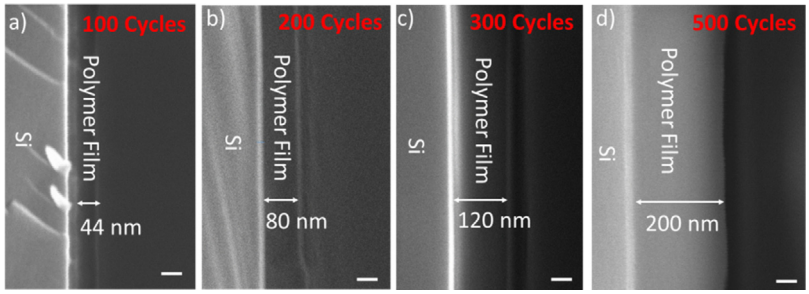

Fig. 2. SEM cross section view of MLD films deposited using a sequence of 1:1 with increasing cycling number. Scale bar represents 50 nm.

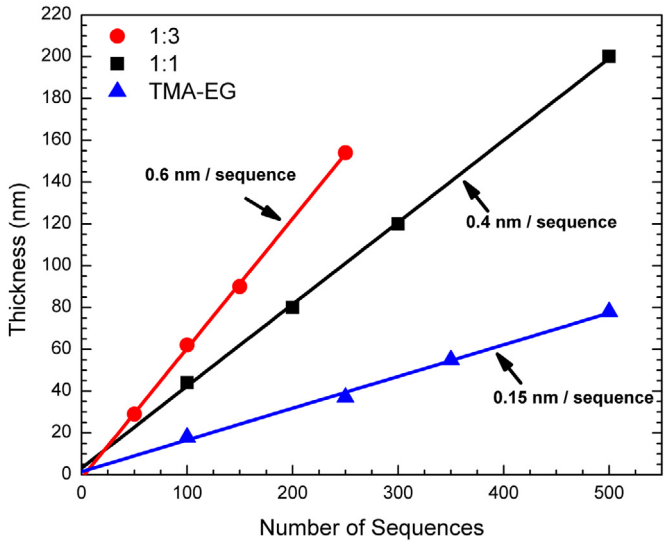

Fig. 3. Thickness of 1:1, 1:3 and TMA-EG MLD films verses number of deposition cycles at 150 °C.

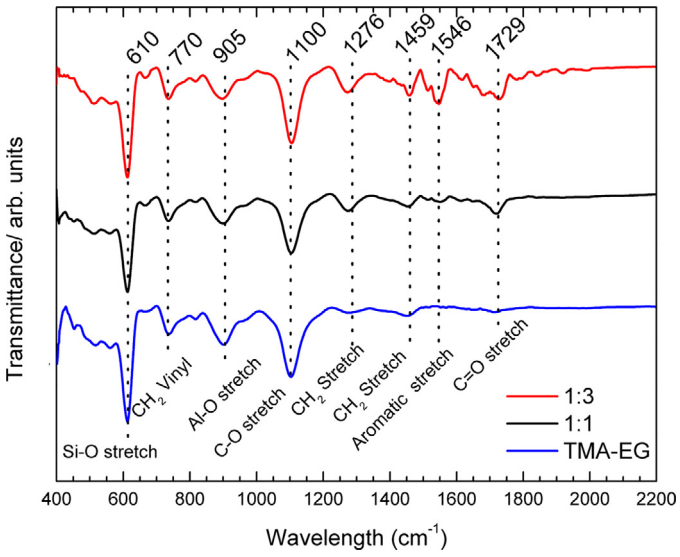

Fig. 4. FTIR spectra for 100 nm thick TMA-EG, 1:1 and 1:3 MLD films deposited on double polished Si at 150 °C.

negligible roughness. Fig. 1 – suggested growth sequence for MLD films with tuneable carbon to aluminum ratio.

Fig. 3 shows the cycle dependence of the deposited MLD films. It is clear that the 1:1 and 1:3 films increase in thickness linearly with MLD cycle number. By fitting the data in Fig. 3 linearly, the growth per cycle of the MLD films is calculated to be 0.4 nm/sequence and 0.6 nm/sequence for 1:1 and 1:3 films, respectively. For comparison, cycles of TMA-EG were also deposited on Si with a growth rate of 0.15 nm/sequence. This value correlates well with previous work [21].

Fig. 4 shows the FTIR spectra for TMA-EG, 1:1 and 1:3 films. All spectra demonstrate a prominent peak at 610 cm^{-1} and 905 cm^{-1} which can be attributed to Si—O and Al—O bonds respectively [22,23]. In addition, C—O stretching vibrations are observed at 1100 cm^{-1} for all spectra, as a result of EG deposition. As expected, additional peaks can be found for the 1:1 and 1:3 film due the inclusion of TC. Typically a strong, C=O absorption band is seen between 1750–1735 cm^{-1} for saturated aliphatic esters. However, the C=O stretch for 1:1 and 1:3 films appears at 1729 cm^{-1}. This stretching vibration is shifted to lower frequency due to its conjugation with an aromatic group [24]. The higher carbon content films also display a weak skeletal vibration due to C—C stretching within the ring with absorptions in the 1450–1550 cm^{-1} region [25]. More importantly, the signature peak for chlorinated C=O and C—Cl are not present in the obtained FTIR spectra, indicating that all TC has been successfully removed from the substrate along with its reaction by-products [26].

Raman spectroscopy was employed to determine the state of carbon after pyrolysis. Pyrolysis was conducted at 1 atm under 5% H_2/Ar gas at various temperatures (600 °C, 700 °C, 800 °C and 900 °C). Fig. 5a and b shows the Raman spectra for pyrolyzed 1:1 and 1:3 MLD films at various temperatures. Two peaks located at ~1350 cm^{-1} and 1590 cm^{-1} appear as a result of pyrolysis and vary in intensity for each sample set. Raman intensities at 1590 cm^{-1} and 1350 cm^{-1} are usually designated as G (graphitic sp^2 phase carbon) and D (disordered sp^2/sp^3 phase carbon), respectively [27]. Obtained Raman spectra for 1:3 MLD films display a narrowing of the G band as well as a slight shift to 1600 cm^{-1} with increasing pyrolysis temperature. This is associated with a growth in size and/or number of nanographitic crystals [28]. This structural change can be attributed to the material becoming polycrystalline as well as a reduction in the number of sp^3 sites [29]. Ferrari et al. [30] demonstrated that the full width at half maximum (FWHM) of the G peak is a measure of graphitic disorder and increases continuously with disorder. Fig. 5b indicates that with increasing temperature, the G peak of the 1:3 film increases in intensity while simultaneously becoming narrower. This is a strong indication that the graphitic planes within the film are increasing in order and size. However, the spectrum for 1:1 MLD films is starkly different. There is a dramatic decrease in both D and G band intensity along with a peak broadening with increasing pyrolysis temperature. This broadening indicates that phonon lifetimes are being significantly reduced, implying that defect density of the sp^2 carbon is increasing [31]. Dillion et al. [28] determined that a decrease in D and G band linewidth is consistent with the removal of bond-angle disorder and increasing dominance of crystallites [28,31,32]. This would suggest that for the 1:1 MLD films, as pyrolysis temperatures increase, bond-angle disorders also increase, resulting in

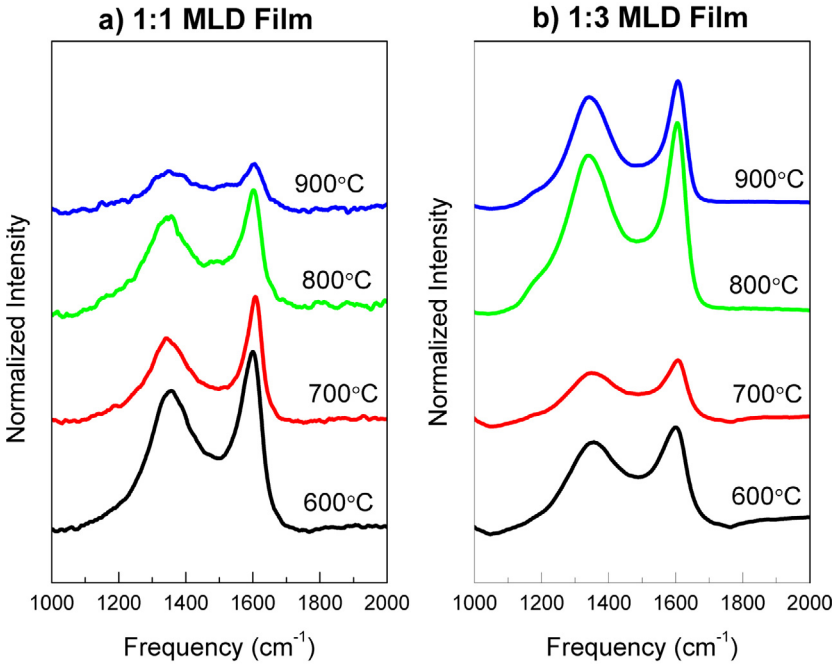

Fig. 5. Raman spectra for (a) 1:1 and (b) 1:3 MLD films with initial thickness of 200 nm annealed with 5% H_2/Ar at 600, 700, 800 and 900 °C for 1 h.

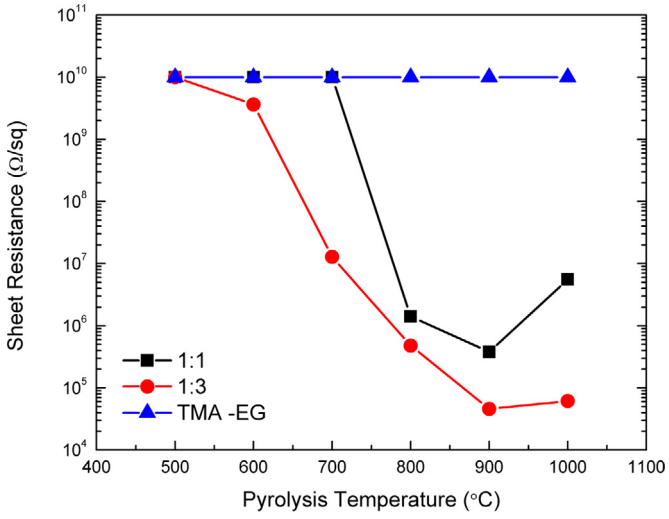

Fig. 6. Sheet resistance measurements for 100 nm thick TMA-EG, 1:1, and 1:3 MLD films pyrolyzed at various temperatures.

increased linewidth in the Raman spectra. Furthermore, a reduction in phonon lifetime may also be attributed to the formation of Al_2O_3.

Sheet resistance of 1:1 and 1:3 MLD deposited films was plotted as a function of heat treatment temperature, as shown in Fig. 6. The films were grown on high purity SiO_2 glass slides and heat treated under a mixture of 5% hydrogen gas and argon at temperatures from 500 to 1000 °C for 1 h. Sheet resistance was obtained using a four point probe. As shown in Fig. 6, sheet resistance rapidly declines until 900 °C. This dramatic decrease in sheet resistance is attributed to the formation of nanocrystalline graphite, as indicated by Raman spectroscopy. Similar evolution in electrical resistance has been observed for the pyrolysis of pure organic polymers [33]. Interestingly, the 1:3 MLD film demonstrates a sheet resistance of 4.6×10^4 Ω/sq compared to 3.5×10^5 Ω/sq for the 1:1 MLD films pyrolyzed at 900 °C. Increasing the carbon content of the film, results in a decrease in sheet resistance. This decrease in sheet resistance is attributed to changes in the film composition as a result of decreasing carbon to aluminum ratio [34]. Furthermore, the significant decrease in sheet resistance for a higher carbon film may also be due to larger domains of nanocrystalline graphite and less disordered carbon. As indicated by Raman spectroscopy, the 1:3 film pyrolyzed at 900 °C displays sharp D and G bands, whereas the 1:1 film pyrolyzed at the same temperature has very broad D and G bands, indicating increased carbon disorder and decreased graphitic nanocrystalline size. Another possibility for the large difference in sheet resistance between the 1:1 and 1:3 film is the possible presence of carbothermally reduced aluminum oxide. Typically carbothermal reduction of alumina occurs at temperatures > 1400 °C. However, previous studies have determined that the formation of Al_4O_4C and Al_4C_3 can occur at much lower temperatures but is highly dependent on Al_2O_3 grain size and reducing environment [35]. Interestingly at temperatures greater than 900 °C, the sheet resistance for both films increases. A similar behavior is also observed in the pyrolysis of other hybrid MLD films [5]. The large increase in sheet resistance at 1000 °C may be attributed to the chemical attack of basic groups in the film by aluminum species. A previous paper published by Bou et al. [36] demonstrated how aluminum preferentially attacks basic sites which may lead to compounds with increased resistance. Another possibility for the occurrence of this phenomenon is the change in film morphology as it begins to shrink and lose uniformity at higher temperatures. This may also result in higher sheet resistant measurements taken by a four point probe. A better understanding of this phenomenon can be determined through the use of current sensing atomic force microscopy along with XPS of the film after annealing at temperatures greater than 1000 °C.

The structure of amorphous materials is difficult to determine with diffraction-based techniques due to the lack of long-range order. To overcome this difficulty, X-ray spectroscopy is employed due to its inherent sensitivity to the local environment of the element to be examined. Furthermore, synchrotron XPS is highly surface sensitive and can provide a stronger signal due to the use of a high intensity light source. As shown in Fig. 7a, the as deposited films have a binding energy of 74.7 eV, 75.0 eV, and 75.6 eV for the 1:3, 1:1 and TMA-EG films respectively. Al—O bonds are typically

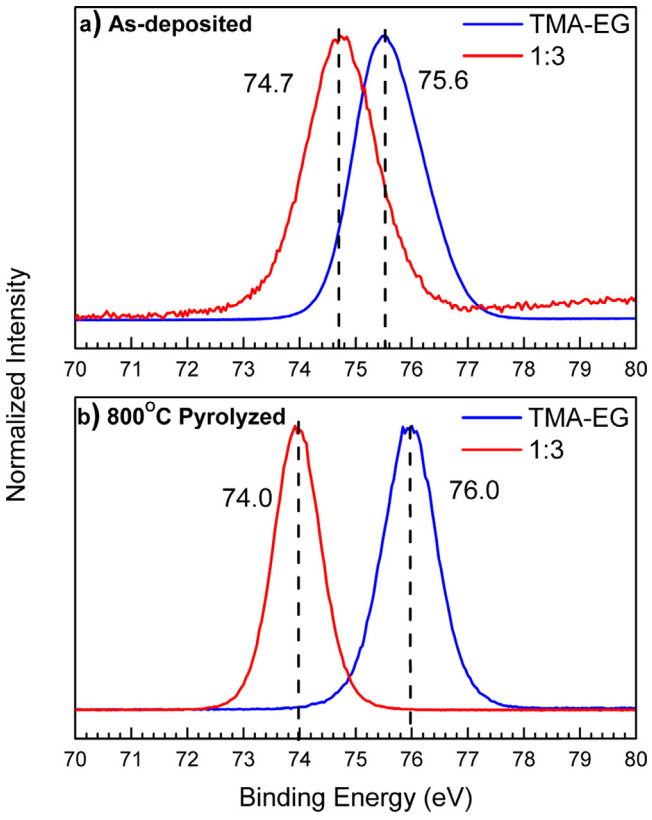

Fig. 7. Synchrotron based XPS of (a) as deposited and (b) 800 °C pyrolyzed TMA-EG and 1:3 MLD films.

seen at 74.6 eV and shift to higher binding energy when in a higher oxidized forms such as Al—O—C [37–39]. This indicates that the aluminum in the TMA-EG films exist at a higher oxidation state than in the 1:1 and 1:3 MLD films. Interestingly, pyrolysis of TMA-EG films results in the aluminum peak shifting to higher binding energy, while the aluminum 1:1 and 1:3 MLD films shift to lower binding energy. The increased binding energy for pyrolyzed TMA-EG shift from 75.6 eV to 76.0 eV is strong evidence that Al_2O_3 is formed. The decrease in binding energy seen for 1:1 and 1:3 films, down to 74.2 eV and 74.0 eV, respectively, is a clear indication that the higher carbon content in the film results in reduction of aluminum. This may also be linked to the decrease seen in sheet resistance observed for pyrolyzed MLD films. The increase in the aluminum 2p peak for TMA-EG films can be attributed to a low carbon to aluminum ratio. However, because the carbon to aluminum ratio is much higher in the 1:1, and even more so in 1:3 MLD films, carbothermal reduction is more likely to occur.

4. Conclusions

Aluminum alkoxide hybrid inorganic–organic films with tuneable carbon content were grown using sequential exposures of TMA, EG and TC. Pure alucone, 1:1 and 1:3 films were then pyrolyzed under a reducing atmosphere to produce a conductive Al_2O_3/carbon composite film. Raman spectra of the pyrolyzed films indicate that carbon content in the film leads to nanocrystalline graphite. The amount of nanocrystalline graphite in the film is related to the amount of carbon deposited. Sheet resistance of pyrolyzed films dramatically decreased with increasing pyrolysis temperature. Furthermore, films produced with higher carbon content resulted in a greater decrease in sheet resistance due increased sp^2 formation. Synchrotron XPS revealed that following pyrolysis, increasing carbon content in aluminum alkoxide films leads to the carbothermal reduction of aluminum. This paper also demonstrates how the capabilities of MLD can be used to create hybrid inorganic–organic films with tuneable composition. Using this novel MLD approach, thin hybrid films with tuneable amorphous polymeric regions and dense inorganic regions can be made. This type of film has a number of applications such as in solid polymer electrolytes for lithium ion batteries which require regions of highly amorphous carbon for elevated lithium ion mobility. Furthermore, using this type of approach may lead to better control over pore size for MLD films annealed in air. By tuning the amount of carbon to aluminum in the film, porous aluminum oxide with various pore sizes can be fabricated.

References

[1] J.H. Noh, S.H. Im, J.H. Heo, T.N. Mandal, S. Il Seok, Chemical management for colorful, efficient, and stable inorganic–organic hybrid nanostructured solar cells, Nano Lett. 13 (2013) 1764–1769, http://dx.doi.org/10.1021/nl400349b.
[2] L. Wang, M.-H. Yoon, G. Lu, Y. Yang, A. Facchetti, T.J. Marks, High-performance transparent inorganic–organic hybrid thin-film n-type transistors, Nat. Mater. 5 (2006) 893–900, http://dx.doi.org/10.1038/nmat1755.
[3] Y. Zou, L. Moreel, H. Lin, J. Zhou, L. Li, S. Danto, et al., Solution processing and resist-free nanoimprint fabrication of thin film chalcogenide glass devices: inorganic–organic hybrid photonic integration, Adv. Opt. Mater. 2 (2014) 759–764, http://dx.doi.org/10.1002/adom.201400068.
[4] H. Ma, R. Gao, D. Yan, J. Zhao, M. Wei, Organic–inorganic hybrid fluorescent ultrathin films and their sensor application for nitroaromatic explosives, J. Mater. Chem. C 1 (2013) 4128, http://dx.doi.org/10.1039/c3tc30142g.
[5] A.I. Abdulagatov, K.E. Terauds, J.J. Travis, A.S. Cavanagh, R. Raj, S.M. George, Pyrolysis of titanicone molecular layer deposition films as precursors for conducting TiO_2/carbon composite films, J. Phys. Chem. C 117 (2013) 17442–17450, http://dx.doi.org/10.1021/jp4051947.
[6] B.H. Lee, B. Yoon, A.I. Abdulagatov, R.a. Hall, S.M. George, Growth and properties of hybrid organic–inorganic metalcone films using molecular layer deposition techniques, Adv. Funct. Mater. 23 (2013) 532–546, http://dx.doi.org/10.1002/adfm.201200370.
[7] G. Larsen, R. Velarde-Ortiz, K. Minchow, A. Barrero, I.G. Loscertales, A method for making inorganic and hybrid (organic/inorganic) fibers and vesicles with diameters in the submicrometer and micrometer range via sol–gel chemistry and electrically forced liquid jets, J. Am. Chem. Soc. 125 (2003) 1154–1155, http://dx.doi.org/10.1021/ja028983i.
[8] X. Wang, C.M. Cho, W.Y. Say, A.Y.X. Tan, C. He, H.S.O. Chan, et al., Organic–inorganic hybrid liquid crystals derived from octameric silsesquioxanes. Effect of the peripheral groups in mesogens on the formation of liquid crystals, J. Mater. Chem. 21 (2011) 5248, http://dx.doi.org/10.1039/c0jm03406a.
[9] V. Singh, T. Naka, S. Takami, A. Sahraneshin, T. Togashi, N. Aoki, et al., Hydrothermal synthesis of inorganic–organic hybrid gadolinium hydroxide nanoclusters with controlled size and morphology, Dalton Trans. 42 (2013) 16176–16184, http://dx.doi.org/10.1039/c3dt51692j.
[10] P.R.L. Malenfant, J. Wan, S.T. Taylor, M. Manoharan, Self-assembly of an organic–inorganic block copolymer for nano-ordered ceramics, Nat. Nanotechnol. 2 (2007) 43–46, http://dx.doi.org/10.1038/nnano.2006.168.
[11] T. Kimura, K. Kato, Synthesis of ordered mesoporous aluminium alkylenediphosphonates with integrated inorganic? Organic hybrid frameworks, J. Mater. Chem. 17 (2007) 559, http://dx.doi.org/10.1039/b612637e.
[12] H. Tachibana, Y. Yamanaka, H. Sakai, M. Abe, M. Matsumoto, Highly conductive inorganic–organic hybrid Langmuir-Blodgett films based on MoS_2, Chem. Mater. 12 (2000) 854–856, http://dx.doi.org/10.1021/cm990664b.
[13] T. Yoshida, J. Zhang, D. Komatsu, S. Sawatani, H. Minoura, T. Pauporté, et al., Electrodeposition of inorganic/organic hybrid thin films, Adv. Funct. Mater. 19 (2009) 17–43, http://dx.doi.org/10.1002/adfm.200700188.
[14] R.L. Puurunen, Surface chemistry of atomic layer deposition: a case study for the trimethylaluminum/water process, J. Appl. Phys. 97 (2005), http://dx.doi.org/10.1063/1.1940727.
[15] B. Yoon, D. Seghete, A.S. Cavanagh, S.M. George, Molecular layer deposition of hybrid organic–inorganic alucone polymer films using a three-step abc reaction sequence, Chem. Mater. 21 (2009) 5365–5374, http://dx.doi.org/10.1021/cm9013267.
[16] D.C. Miller, R.R. Foster, S.H. Jen, J.a. Bertrand, D. Seghete, B. Yoon, et al., Thermomechanical properties of aluminum alkoxide (alucone) films created using molecular layer deposition, Acta Mater. 57 (2009) 5083–5092, http://dx.doi.org/10.1016/j.actamat.2009.07.015.
[17] J. Liu, B. Yoon, E. Kuhlmann, M. Tian, J. Zhu, S.M. George, et al., Ultralow thermal conductivity of atomic/molecular layer-deposited hybrid organic–inorganic zincone thin films, Nano Lett. 13 (2013) 5594–5599, http://dx.doi.org/10.1021/nl403244s.
[18] J.J. Brown, R.a. Hall, P.E. Kladitis, S.M. George, V.M. Bright, Molecular layer deposition on carbon nanotubes, ACS Nano 7 (2013) 7812–7823, http://dx.doi.org/10.1021/nn402733g.

[19] X. Liang, A.W. Weimer, An overview of highly porous oxide films with tunable thickness prepared by molecular layer deposition, Curr. Opin. Solid State Mater. Sci. 19 (2014), http://dx.doi.org/10.1016/j.cossms.2014.08.002.
[20] C. Chen, P. Li, G. Wang, Y. Yu, F. Duan, C. Chen, et al., Nanoporous nitrogen-doped titanium dioxide with excellent photocatalytic activity under visible light irradiation produced by molecular layer deposition, Angew. Chemie – Int. Ed. 52 (2013) 9196–9200, http://dx.doi.org/10.1002/anie.201302329.
[21] A.A. Dameron, D. Seghete, B.B. Burton, S.D. Davidson, A.S. Cavanagh, J.A. Bertrand, et al., Molecular layer deposition of alucone polymer films using trimethylaluminum and ethylene glycol, Chem. Mater. 20 (2008) 3315–3326, http://dx.doi.org/10.1021/cm7032977.
[22] G.L. Fisher, A.V. Walker, A.E. Hooper, T.B. Tighe, K.B. Bahnck, H.T. Skriba, et al., Bond insertion, complexation, and penetration pathways of vapor-deposited aluminum atoms with HO- and CH_3O-terminated organic monolayers, J. Am. Chem. Soc. 124 (2002) 5528–5541, http://dx.doi.org/10.1021/ja0123453.
[23] M. Nakamura, Y. Mochizuki, K. Usami, Y. Itoh, T. Nozaki, Infrared absorption spectra and compositions of evaporated silicon oxides (SiOx), Solid State Commun. 50 (1984) 1079–1081, http://dx.doi.org/10.1016/0038-1098(84)90292-8.
[24] D. Pavia, G. Lampman, G. Kris, J. Vyvyan, Introduction to Spectroscopy, 4th ed., Brooks/Cole, Belmont, 2009, pp. 66–69.
[25] T.V. Ivanova, P.S. Maydannik, D.C. Cameron, Molecular layer deposition of polyethylene terephthalate thin films, J. Vac. Sci. Technol. A Vacuum Surf. Film. 30 (2012) 01A121, http://dx.doi.org/10.1116/1.3662846.
[26] N.M. Adamczyk, A.A. Dameron, S.M. George, Molecular layer deposition of poly(p-phenylene terephthalamide) films using terephthaloyl chloride and p-phenylenediamine, Langmuir 24 (2008) 2081–2089, http://dx.doi.org/10.1021/la7025279.
[27] M.a. Tamor, W.C. Vassell, Raman "fingerprinting" of amorphous carbon films, J. Appl. Phys. 76 (1994) 3823–3830, http://dx.doi.org/10.1063/1.357385.
[28] R. Dillon, J. Woollam, V. Katkanant, Use of Raman scattering to investigate disorder and crystallite formation in as-deposited and annealed carbon films, Phys. Rev. B 29 (1984) 3482–3489, http://dx.doi.org/10.1103/PhysRevB.29.3482.
[29] A. Ferrari, J. Robertson, Interpretation of Raman spectra of disordered and amorphous carbon, Phys. Rev. B 61 (2000) 14095–14107, http://dx.doi.org/10.1103/PhysRevB.61.14095.
[30] A. Ferrari, S. Rodil, J. Robertson, Interpretation of infrared and Raman spectra of amorphous carbon nitrides, Phys. Rev. B 67 (2003) 1–20, http://dx.doi.org/10.1103/PhysRevB.67.155306.
[31] R.G. Buckley, T.D. Moustakas, L. Ye, J. Varon, Characterization of filament-assisted chemical vapor deposition diamond films using Raman spectroscopy, J. Appl. Phys. 66 (1989) 3595–3599, http://dx.doi.org/10.1063/1.344065.
[32] J. Gonzalez-Hernandez, G.H. Azarbayejani, R. Tsu, F.H. Pollak, Raman, transmission electron microscopy, and conductivity measurements in molecular beam deposited microcrystalline Si and Ge: a comparative study, Appl. Phys. Lett. 47 (1985) 1350–1352, http://dx.doi.org/10.1063/1.96277.
[33] Z. Sun, X. Shi, X. Wang, Y. Sun, Structure and properties of hard carbon films depending on heat treatment temperatures via polymer precursor, Diam. Relat. Mater. 8 (1999) 1107–1113, http://dx.doi.org/10.1016/S0925-9635(99)00009-6.
[34] R. Kostecki, B. Schnyder, D. Alliata, X. Song, K. Kinoshita, R. Kötz, Surface studies of carbon films from pyrolyzed photoresist, Thin Solid Films 396 (2001) 36–43, http://dx.doi.org/10.1016/S0040-6090(01)01185-3.
[35] I. Ahmad, M. Unwin, H. Cao, H. Chen, H. Zhao, A. Kennedy, et al., Multi-walled carbon nanotubes reinforced Al_2O_3 nanocomposites: mechanical properties and interfacial investigations, Compos. Sci. Technol. 70 (2010) 1199–1206, http://dx.doi.org/10.1016/j.compscitech.2010.03.007.
[36] M. Bou, J.M. Martin, T. Le Mogne, L. Vovelle, Chemistry of the interface between aluminium and polyethyleneterephthalate by XPS, Appl. Surf. Sci. 47 (1991) 149–161, http://dx.doi.org/10.1016/0169-4332(91)90029-J.
[37] R. Cueff, G. Baud, M. Benmalek, J. Besse, J. Butruille, M. Jacquet, X-ray photoelectron spectroscopy studies of plasma-modified PET surface and alumina/PET interface, Appl. Surf. Sci. 115 (1997) 292–298, http://dx.doi.org/10.1016/S0169-4332(96)01089-6.
[38] R. Cueff, G. Baud, M. Benmalek, J.P. Besse, J.R. Butruille, M. Jacquet, Alumina coatings on polyethylene terephthalate: characterisation and X-ray photoelectron spectroscopy study, Surf. Coat. Technol. 80 (1996) 96–99, http://dx.doi.org/10.1016/0257-8972(95)02692-4.
[39] B. Maruyama, F.S. Ohuchi, L. Rabenberg, Catalytic carbide formation at aluminium–carbon interfaces, J. Mater. Sci. Lett. 9 (1990) 864–866, http://dx.doi.org/10.1007/BF00720185.